Atmospheric Research 92 (2009) 443–454

Contents lists available at ScienceDirect

Atmospheric Research

journal homepage: www.elsevier.com/locate/atmos

Particulate contribution to extinction of visible radiation: Pollution, haze, and fog

Thierry Elias [a,*], Martial Haeffelin [a], Philippe Drobinski [a], Laurent Gomes [b], Jerome Rangognio [b], Thierry Bergot [b], Patrick Chazette [c], Jean-Christophe Raut [c], Michèle Colomb [d]

[a] LMD/IPSL, Ecole Polytechnique, 91128 Palaiseau, France
[b] CNRM/Météo-France, 41 Av Coriolis, 31057 Toulouse, France
[c] LSCE/IPSL, Orme des Merisiers Bât. 701, 91191 Gif Sur Yvette, France
[d] LRPC, 8-10 rue Bernard Palissy, 63017 Clermont-Ferrand, France

ARTICLE INFO

Article history:
Received 24 September 2008
Received in revised form 19 December 2008
Accepted 14 January 2009

Keywords:
Fog
Aerosol
Particle
Droplets
Size distribution
Extinction coefficient

ABSTRACT

A data set acquired by eight particle-dedicated instruments set up on the SIRTA (Site Instrumental de Recherche par Télédétection Atmosphérique, which is French for Instrumented Site for Atmospheric Remote Sensing Research) during the ParisFog field campaign are exploited to document microphysical properties of particles contributing to extinction of visible radiation in variable situations. The study focuses on a 48-hour period when atmospheric conditions are highly variable: relative humidity changes between 50 and 100%, visibility ranges between 65 and 35 000 m, the site is either downwind the Paris area either under maritime influence. A dense and homogeneous fog formed during the night by radiative cooling. In 6 h, visibility decreased down from 30 000 m in the clear-sky regime to 65 m within the fog, because of advected urban pollution (factor 3 to 4 in visibility reduction), aerosol hydration (factor 20) and aerosol activation (factor 6). Computations of aerosol optical properties, based on Mie theory, show that extinction in clear-sky regime is due equally to the ultrafine modes and to the accumulation mode. Extinction by haze is due to hydrated aerosol particles distributed in the accumulation mode, defined by a geometric mean diameter of 0.6 μm and a geometric standard deviation of 1.4. These hydrated aerosol particles still contribute by $20 \pm 10\%$ to extinction in the fog. The complementary extinction is due to fog droplets distributed around the geometric mean diameter of 3.2 μm with a geometric standard deviation of 1.5 during the first fog development stage. The study also shows that the experimental set-up could not count all fog droplets during the second and third fog development stages.

1. Introduction

Particles in suspension in the atmosphere, as aerosol particles and cloud or fog droplets, are responsible for reduction of the visibility range, by scattering and absorbing electromagnetic radiation in the visible wavelengths. Scattering and absorption properties depend on particle number and properties (e.g. size, shape). Strong gradients of visibility are related to both dynamic and thermodynamic processes that occur at spatial and temporal fine-scale resolutions, and which both modify particle number and size. For example, condensation of atmospheric water on aerosol particles modifies their size over two steps. Dry aerosol particles become wet aerosol particles through hydration, when the relative humidity is larger than the deliquescence point (e.g. Winkler, 1988), and aerosol particles are activated to droplets when the atmosphere is saturated in humidity (e.g. Jiusto, 1981). Reduced visibility events have different

* Corresponding author. LMD, Ecole Polytechnique, 91128 Palaiseau, France. Tel.: +33 1 69 33 51 47; fax: +33 1 69 33 51 08.
E-mail address: thierry.elias@lmd.polytechnique.fr (T. Elias).

0169-8095/$ – see front matter © 2009 Published by Elsevier B.V.
doi:10.1016/j.atmosres.2009.01.006

origins, such as urban and industrialized pollution aerosol particles which dim the sky in large cities, such as dust particles downwind desert regions, and such as fogs that are the most critical phenomena in terms of visibility reduction in Europe.

Fog occurrence is predicted according to Numerical Weather Prediction models, with the objective to reduce hazards in transport activities. For example, for road weather, it is crucial to predict rapid gradients in the visibility range down to 50 m. However, Numerical Weather Prediction models usually lack accuracy in prediction of location and time of fog formation and dissipation, as well as in fog density magnitude and heterogeneity. On the one hand, the critical processes occur at fine scales that are unresolved by forecast models and must hence be parameterised. On the other hand, current knowledge is sometimes insufficient to model physical processes, as those related to aerosol microphysical properties, e.g. the radiative transfer in the atmosphere, the dew deposition, as well as the visibility range.

ParisFog is a 6-month field measurement campaign dedicated to study the implication of thermodynamic, dynamic and radiative processes in the fog life cycle, in correlation with microphysical and optical properties of the aerosol particles and fog droplets (Bergot et al., 2008). ParisFog took place during the 2006–2007 winter on the SIRTA (Site Instrumental de Recherche par Télédétection de Atmosphérique, which is French for Instrumented Site for Atmospheric Remote Sensing Research) (Haeffelin et al., 2005), located in a suburban environment 20 km South West of Paris, under two predominant and contrasted influences: maritime by West winds and urban by North–East winds.

Aerosol-dedicated measurements performed over 48 h are analysed as a case study. Eight instruments are dedicated to describe independently the particle microphysical and optical properties. Four particle counters are complementary to provide the size distribution from 0.004 to 40 μm diameter. Particle extinction and aerosol scattering properties are documented with two visibilimeters, a sun-photometer and a nephelometer. The objective of the study is to identify particle populations contributing to light extinction, in variable atmospheric conditions. Jiusto (1981) suggested the significant contribution to fog extinction by wet aerosol particles of the accumulation mode, of diameter smaller than 2 to 4 μm, which are showed by Eldridge (1966) to be predominant in number. To our knowledge, quantitative contribution of these wet aerosol particles in light extinction by fog has not yet been estimated, as Gultepe et al. (2006) point out recently the need to perform measurements of particle size distribution at sizes smaller than 2 μm. Our study focuses on surveying contribution to extinction by accumulation mode particles, relatively to ultrafine aerosol particles in clear-sky conditions and relatively to droplets in fog conditions.

Randriamiarisoa et al. (2006) analysed measurements acquired by nephelometer and particle counters set up nearby SIRTA in the 1998 and 1999 summers during the ESQUIF (Etude et Simulation de la QUalité de l'Air en Ile de France) experiment (Vautard et al., 2003), to propose a parameterisation of the hydration process. As characteristics of the aerosol particles larger than 0.8 μm could not be retrieved with precision, the experimental set-up was enriched for ParisFog by independent measurements of the visibility range to: 1) validate the measured ambient particle size distribution; and 2) identify contribution by accumulation mode particles to extinction in clear-sky and hazy conditions. Moreover the wind components are surveyed to study the effect of dynamic processes on aerosol properties. We also study the effect of aerosol activation on atmospheric extinction by extending measured particle size domain up to 40 μm diameter. Independent measurements of visibility give the opportunity to validate fog size distributions, as has been done by Yuskiewicz et al. (1998), who generate ambient size distributions after applying humidification parameterisation on measurements made in dry conditions during the CHEMDROP field campaign in the Po Valley (Fuzzi et al., 1998). In contrast, ParisFog air samples were deliberately not heated, in order to obtain a consistent data base depending on a minimum of assumptions. Pollution measured in the case study reached levels similar to what is observed in the Po Valley (Noone et al., 1992; Yuskiewicz et al., 1998).

We describe some microphysical and optical properties of the particles contributing to extinction of visible radiation, during clear-sky, pollution, haze and fog events which occurred during the case study, according to the thermodynamic and dynamic processes, and we verify the quality of the experimental set-up. Extinction and scattering coefficients are computed according to Mie theory applied on measurements of the particle size distributions. Computations are compared to independent measurements of the particle optical properties. Section 2 describes the experimental set-up, the case study, and Section 3 the methodology to interpret particle contribution to extinction as a function of the size. Section 4 defines the aerosol properties in clear-sky conditions and Section 5 in the haze regime. Section 6 focuses on particle properties, from ultrafine aerosol particles to droplets, all present during the fog regime. Section 7 provides the conclusion.

2. The experiment

2.1. Experimental set-up of the ParisFog experiment

The ParisFog field experiment took place on the 3 SIRTA observatory platforms (Haeffelin et al., 2005) distributed on a 1×1 km area on the Saclay Plateau, located in a suburban area 20 km South West of Paris (Bergot et al., 2008). SIRTA is usually either under maritime influence either downwind the Paris urban pollution. From November 2006 to April 2007 an ensemble of instruments simultaneously monitored dynamic, thermodynamic and radiative processes in correlation to microphysical properties of aerosol particles and fog droplets. Because fog formation and dissipation is difficult to predict accurately, automatic acquisition in a routine mode was favoured. The instrumental equipment was augmented by manual-operating apparatus during several intensive observation periods (Bergot et al., 2008).

Table 1 lists the instruments considered in this study. Temperature and humidity profiles were monitored by standard sounders located on 2 30-m masts less than 1 km apart. Uncertainty is few % on relative humidity measurements, increasing when relative humidity is larger than 90%.

Table 1
ParisFog instrumental set up used for the 18–19/02 case study (#13 IOP).

Instrument	Model	Domain of sensitivity	Parameter	Temporal resolution	Sampling conditions	Long-term routine
Thermometer and humidity sensor			Temperature and relative humidity	1 min	Ambient outdoor	Yes
Sonic anemometer			Wind speed and direction	1 s	Ambient outdoor	No
Sun/sky-photometer	CIMEL CE318	440, 670, 870, 1020 nm wavelengths	Aerosol optical thickness	15 min	Ambient outdoor	Yes
Visibilimeter	Degreanne DF320	490–750 nm wavelength with a max at 550 nm	Visibility	10 s	Ambient outdoor	No
Visibilimeter	Degreanne DF20+	490–750 nm wavelength with a max at 550 nm	Visibility	10 s	Ambient outdoor	No
Nephelometer	TSI 3563	450, 550, 700 nm wavelengths	Aerosol scattering coefficient	1 min	PM10 inlet downstream	No
Particle counter	PALAS WELAS-2000	0.39–42 μm particle diameter	Aerosol and droplet number per unit of air volume, in 65 size bins	5 min	Ambient outdoor	No
Particle counter	TSI SMPS	0.01–0.50 μm particle diameter	Aerosol number per unit of air volume, in 108 size bins	10 min	PM10 inlet downstream	No
Particle counter	GRIMM CPC-5400	0.004–3 μm particle diameter	Integrated particle number, per unit of air volume	1 min	PM10 inlet downstream	No

SMPS: Scanning Mobility Particle Sizer.
CPC: Condensation Particle Counter.

Particle optical property measurements in the visible spectrum were carried out by several instruments. A CE318 CIMEL sun-photometer operated in the AERONET framework (Holben et al., 1998). It measured aerosol optical thickness at four wavelengths during the day and under cloud-free sky. Two Degreanne visibilimeters (DF320 and DF20+) were operated near the ground (4-m height), on 2 platforms. The instrument provided horizontal visibility range and particle extinction at 550 nm, with a 10–25% uncertainty. Both instruments agreed over a large range of values, except for rare outliers which are the expression of rare spatial heterogeneity in the surface atmospheric layer. A TSI-3563 integrating nephelometer provided the aerosol scattering coefficient $\sigma^{N}_{scat}(\lambda)$ at the 450, 550 and 700 nm wavelengths, with an experimental uncertainty of 10% (Anderson et al., 1996). Scattered light was measured from an air sample downstream a PM10 inlet. Data was not corrected for angular truncation in forward and backward directions.

Particle counting measurements were carried out in parallel by two instruments installed downstream the PM10 inlet. A GRIMM CPC instrument (Aerosol Technik, Model 5400) counted the total aerosol number (cm^{-3}) integrated over the 0.004–3 μm diameter range, with a 10% uncertainty on aerosol number. A TSI SMPS particle counter provided the number of aerosol particles distributed over 108 size bins from 0.01 to 0.50 μm diameter, with 20% accuracy on particle number in each size bin. The particle counter was calibrated before the field campaign by using known concentration of ammonium sulphate particles.

These measurements were complemented by two PALAS WELAS-2000 particle spectrometers sampling directly into the air, that each determine size and number of aerosol particles and fog droplets, in the 0.39–42 μm diameter range, with 20% uncertainty on particle number, per size bin. Raw count measurements provided by the WELAS-2000 are multiplied by a factor to obtain the particle number per air volume unit. The factor represents the volume fraction of the sampled air sounded by the optical system. The sounded air volume depends on the air flow through the optical chamber, the size of the lighted region, and the acquisition time duration. For the case study, a hybrid configuration was adopted, consisting of the optical head of one of the two spectrometers mounted with the electronic acquisition system of the other spectrometer. In this configuration, any of the manufacturer values for the sample volume factor cannot be used. DF320 measurements being considered as a constraint to calibrate the WELAS-2000 instrument, next sections show that measurements are consistent most of the time with a sounded sample volume factor set to 1. Both WELAS-2000 instruments were revised by the manufacturer during the field campaign and were size calibrated with latex particles.

2.2. The case study: 18–19 February 2007

48-hour time series of measurements of temperature (Fig. 1), horizontal visibility (Fig. 2) and particle number (Fig. 3) measured on 18 and 19 February 2007 indicate that the case study concerns a dense and homogeneous fog formed from nocturnal radiative cooling in a polluted environment. The case study corresponds to the #13 intensive observation period (Haeffelin et al., in preparation). Fig. 1 shows the effect of radiative cooling on the temperature vertical profile from the 1500 UT maximum of around 15 °C. Simultaneously, the relative humidity starts to increase from around 50% until fog outbreak, which occurs at around 2300 UT. The radiative cooling (temperature decreased by 10 °C in 8 h) is stopped by the fog where the temperature stays constant and uniform (up to 30 m above ground level (agl)) for around 10 h. Fog extinction seems uniform on the site domain, as measurements by both visibilimeters agree (Fig. 2). Visibility is smaller than 900 m in the fog, while it was around 30 000 m at 1700 UT. Aerosol number N_C measured by the CPC suddenly increased by a factor 3 in the afternoon (Fig. 3), indicating fog formed in a polluted environment ($N_C = 18\,000\ cm^{-3}$ at around 2200 UT).

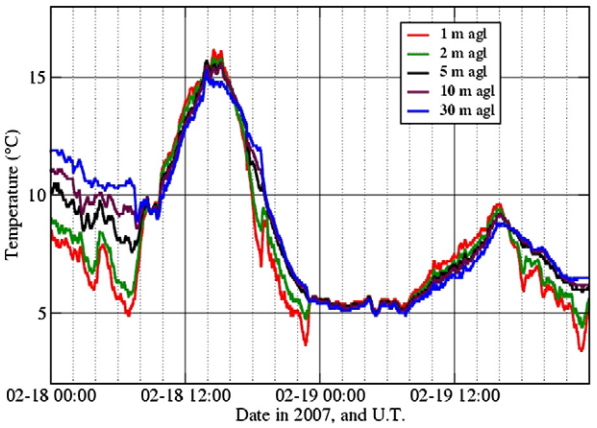

Fig. 1. 48-hour time series of instantaneous 1-min values of temperature (°C), measured at 5 heights on the meteorological mast.

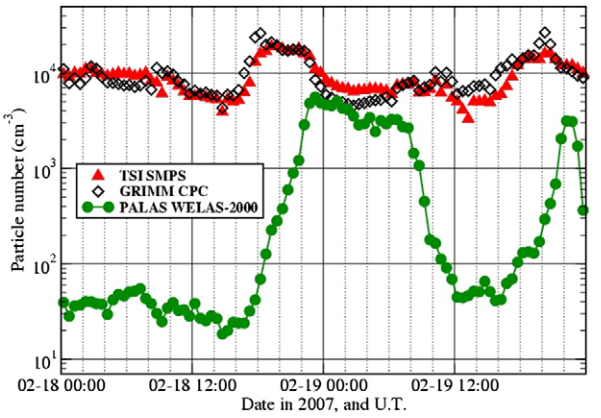

Fig. 3. Time series of 30-minute averaged values of the number of particles per unit volume, either directly measured by the CPC, either integrated from size distributions measured by the SMPS and the WELAS-2000 particle counters (Eq. (1)).

The atmospheric conditions may be classified into 3 regimes according to the visibility measurements: clear-sky, fog, and haze (Table 2). Classification is usually done based on absolute values of the visibility range (e.g. Tardif and Rasmussen, 2007): visibility smaller than 1000 m usually refers to fog (NOAA, 1995), but as is commented by Jiusto (1981) such classification is mostly arbitrary. Another criterion is chosen here to identify the mist transition phase (Eldridge, 1969; Heintzenberg et al., 1998) defined by the start of the aerosol activation process. Aerosol activation is engaged when relative humidity exceeds a threshold value, causing sudden formation of droplets which are the main providers of the particle surface area interacting with visible electromagnetic radiation. Consequently sharp decrease of visibility characterises the mist transition phase. The temporal gradient of visibility is computed to delineate precisely the time interval of the fog regime. Computation is restricted to visibility smaller than 2000 m, as droplets appear at visibility between 1400 and 2000 m according to Meyer et al. (1980), and as Eldridge (1969) situates the mist phase below 1000 m.

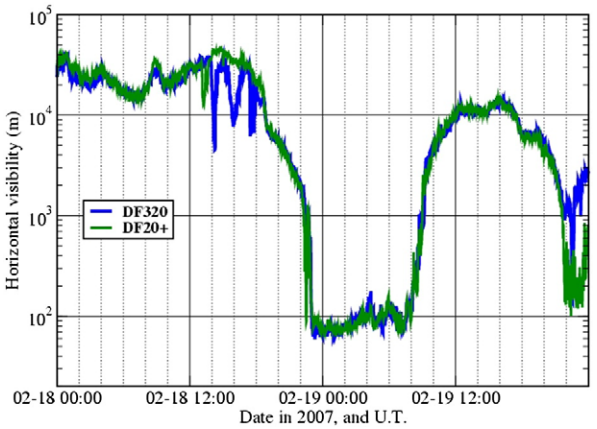

Fig. 2. Time series of the instantaneous 10-s values of the horizontal visibility (m), directly measured by both DF320 and DF20+ visibilimeters, located 1 km apart.

1) Clear-sky regime is defined for visibility values larger than 5000 m. The clear-sky regime lasts for around 30 h over the 48-hour time period: from 0000 to 2020 UT on 18 February and from 1025 to 2010 UT on 19 February. Visibility reaches its maximum value of 35000 m around 1345 UT on 18 February while it stays smaller than 14000 m on 19 February.
2) Fog regime is defined between minimum and maximum in the temporal gradient of visibility, which is computed from the 10-second temporal resolution measurements. Maximum of temporal gradient, in negative values (−140%/min), is reached at 2245 UT for a visibility of around 400 m. Visibility stabilizes 20 min later with values smaller than 80 m. Maximum of temporal gradient, in positive values (150%/min), is reached at 0845 UT during the dissipation phase, for a visibility of 880 m. Fog lasts for around 10 h during the case study. The fog is dense with an averaged visibility of 100 ± 45 m, smaller than 190 ± 132 m, as observed by Heintzenberg et al. (1998). Fog formed during the first part of the 19–20 February night comparatively presents high heterogeneity in time and space. Both visibilimeters disagree in terms of visibility, and according to the DF320 instrument, the fog lasts only 10 min, around 2230 UT, with visibility smaller than 400 m. This fog will not be described in detail in the paper.
3) As haze regimes occur as transition between the clear-sky and fog regimes, visibility is highly variable in this regime. Haze regime is defined as visibility smaller than 5000 m, down until fog occurrence. On 18 February, the haze regime starts at 2020 UT and lasts until 2245 UT. On 19 February morning, fog dissipates into a haze at 0845 UT that lasts until 1025 UT. Haze forms again at 2010 UT 19/02 and lasts until 2230 UT according to the DF320 instrument. Visibility is reduced by a factor larger than 10 within less than 3 h, in the pre-fog haze of 18/02 and 19/02 evenings, and is increased by a factor 5 in 90 min in the 18/02 morning post-fog haze.

The visibility values of 400 m and 880 m characterising the mist transition phase, between fog and haze regimes, are

Table 2
Characterisation of the three clear-sky, haze and fog regimes, in terms of duration, visibility, relative humidity and particle properties.

Regime	Time period (UT)	Time duration	DF320		Relative humidity (%)	SMPS		WELAS-2000			
			Visibility (m)	Extinction coefficient (Mm^{-1})		Ultrafine particle number (cm^{-3})	Ultrafine mode extinction (Mm^{-1})	Accumulation particle number (cm^{-3})	Accumulation mode extinction (Mm^{-1})	Fog droplet number (cm^{-3})	Fog droplet mode extinction (Mm^{-1})
Clear-sky	0000–2021 18/02	20:21	5000–35 000	70–580	50–90	3900–19 000	20–130	20–400	30–500	0	0
	1023–2008 19/02	9:45	5000–14 000	205–580	78–95	3000–17 000	40–80	40–310	50–300	0	0
Haze	2021–2247 18/02	2:16	400–5000	580–7500	90–100	15 300–17 800	100–130	400–5200	500–11 100	0	0
	0843–1023 19/02	1:40	880–5000	580–3400	90–100	6200–8300	60–70	120–1140	200–1260	0	0
	2008–2228 19/02	2:20	330–5000	580–9000	90–100	12 100–15 800	110–130	300–3200	300–6000	0	0
	2238–2400 19/02	1:22	390–5000	580–7600	90–100	10 300–11 600	120–150	380–3200	440–6500	0	0
Fog	2247 18/02–0843 19/02	09:56	65–880	3400–43 000	100	6000–11 400	60–130	1100–5700	1300–13 200	3–700	50–19 300
	2228–2238 19/02	0:10	140–390	10 000–21 000	90–100	15 000	150	3200	6500		1800

Extinction coefficient is computed at 550 nm.

consistent with the 500–1000 m visibility interval fixed by Eldridge (1969) and used by Heintzenberg et al. (1998). Fog life cycle and clear-sky regime may also be described in terms of particle numbers, which are plotted in Fig. 3. Particle number is computed as

$$N = \sum_{D_{\min}}^{D_{\max}} \Delta n(D) \tag{1}$$

where $\Delta n(D)$ represents the size distribution, i.e. the particle number (cm^{-3}) measured per size bin around the diameter D, per air volume unit, and that is provided by several instruments. N_S is derived from the SMPS measurements, with $D_{min} = 0.01$ μm and $D_{max} = 0.50$ μm. N_W is calculated from WELAS-2000 measurements with $D_{min} = 0.39$ μm and $D_{max} = 42$ μm. WELAS-2000 detects changes of regimes, consistently with visibilimeters. N_W is smaller than 60 cm^{-3} until 1745 UT 18/02 and then starts to increase (Fig. 3), simultaneously to the decrease of the visibility range (Fig. 2). A plateau of values larger than 4500 cm^{-3} is reached from 2245 UT, corresponding to the time of the fog outbreak. Values decrease back under 100 cm^{-3} from 1115 UT to 1715 UT 19/02. N_S is compared to the particle number N_C, directly measured by the CPC (Fig. 3). Number of particles larger than 0.50 μm, downstream the inlet, is negligible, as N_S and N_C generally agree within added uncertainty. Both CPC and SMPS indicate the background level of pollution where the fog is formed. Section 3 describes the methodology for quantitative comparisons of measured visibility with computations, performed in Sections 4, 5 and 6, for the three regimes.

3. The methodology

Microphysical measurements are used to estimate aerosol optical properties for validating the measurement set and to compute contribution to extinction by different particle populations. More specifically, ambient particle size distributions are generated from measurements made by the SMPS and WELAS-2000 particle counters, and the extinction coefficient is used as intercomparison parameter. Modes in the size distributions are identified and are isolated to estimate contribution to extinction by different particle populations. The methodology is described thereafter. The data temporal resolution is harmonised using 30-minute averages.

3.1. Microphysical properties

The particle size distribution in ambient conditions is generated by joining SMPS (from 0.01 to 0.39 μm) to WELAS-2000 (beyond 0.39 μm) measurements. Time series of the ambient particle size distribution $\frac{\Delta n(D)}{\Delta \ln D}$ is plotted in Fig. 4a, and time series of the equivalent volume size distribution $\frac{\Delta n(D)}{\Delta \ln D}\frac{\pi D^3}{6}$ is plotted in Fig. 4b. According to Fig. 4, the accumulation mode is included between 0.4 and 2 μm, which is consistent with literature: Kunkel (1984) observes a discontinuity in fog size distribution at 2.5 μm; according to Noone et al. (1992), accumulation mode aerosols are included between 0.1 and 2.5 μm diameter, while Seinfeld and Pandis (1998) limit upper bound at 1 μm. SMPS sounds the Aitken mode as well as the nucleation mode, which both

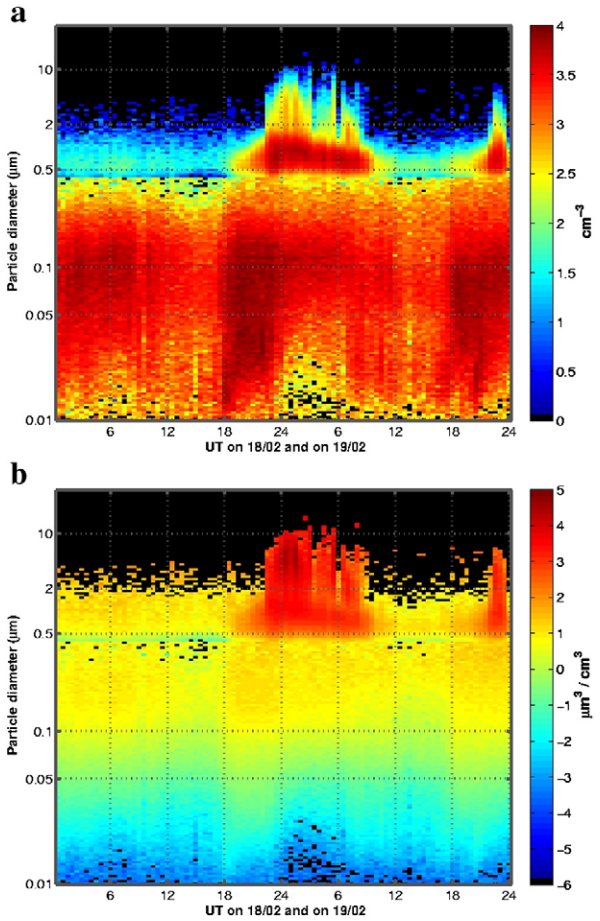

Fig. 4. a. 48-hour time series of the ambient number size distribution $\frac{\Delta n(D)}{\Delta lnD}$ (cm^{-3}) generated from SMPS and WELAS-2000 measurements, on a 10-logarithmic scale. Fig. 4b. As Fig. 4a but for the volume size distribution $\frac{\Delta n(D)}{\Delta lnD}\frac{\pi D^3}{6}$ (μm^3 cm^{-3}).

compose the ultrafine aerosol particles (Seinfeld and Pandis, 1998; Yuskiewicz et al., 1998). In the following, we will associate N_S to the ultrafine aerosol number. WELAS-2000 measurements are used to provide the accumulation mode aerosol number N_{acc}, using Eq. (1) with $D_{min}=0.4$ µm and $D_{max}=2$ µm, as well as the fog droplet number N_{fd}, with $D_{min}=2$ µm and $D_{max}=42$ µm. Particle number size distributions are approximated by multimodal log-normal distributions (Heintzenberg, 1994). Each instrument, i.e. SMPS or WELAS-2000, provides six parameters (Table 3) describing a bimodal size distribution:

$$\frac{dn(D)}{dlnD}=\frac{N_1}{s_{g,1}\sqrt{2\pi}}e^{-\frac{1}{2}\left(\frac{\left(ln\frac{D}{D_{g,1}}\right)}{lns_{g,1}}\right)^2}+\frac{N_2}{s_{g,2}\sqrt{2\pi}}e^{-\frac{1}{2}\left(\frac{\left(ln\frac{D}{D_{g,2}}\right)}{lns_{g,2}}\right)^2} \quad (2)$$

$D_{g,1/2}$ are the geometric mean diameters for the modes 1 and 2, $s_{g,1/2}$ are the geometric standard deviations for the two modes, $N_{1/2}$ represent the mode number concentrations. Results of the fitting procedure are manually checked to ensure the physical meaning of the size distribution parameters.

3.2. Optical properties

The extinction coefficient σ^K_{ext} is retrieved from the measured horizontal visibility range, according to the Koschmieder Equation (Koschmieder, 1925, and e.g. Hess et al., 1998):

$$\sigma^K_{ext}=\frac{-ln(C_V)}{\text{visibility}} \quad (3)$$

C_V is the visual contrast, defined at 5% for the two visibilimeters. σ^K_{ext} is retrieved at 550 nm, and is expressed in Mm^{-1} (10^{-6} m^{-1}). The extinction coefficient σ^M_{ext} is also derived at 550 nm, from the measured size distribution, according to Mie theory applicable to spherical aerosol particles (e.g. Bohren and Huffman, 1983):

$$\sigma^M_{ext}=\sum_{D_{min}}^{D_{max}}\frac{\pi D^2}{4}\Delta n(D)Q_{ext}(m,D) \quad (4a)$$

$Q_{ext}(m, D)$ is the Mie extinction efficiency factor that depends on the particle size and the refractive index m which is assumed to be independent on wavelength and time. AERONET provides an indicative value of the aerosol refractive index (Holben et al., 1998) for the SIRTA on 18 February, $m=1.55-0.01i$. The real part is consistent with the conditions of a dry atmosphere (Shettle and Fenn, 1979) and the imaginary part indicates presence of absorbing particles typical of urban and industrialized pollution (Shettle and Fenn, 1979). $m=1.55-0.01i$ is used for aerosol particles of diameter smaller than 2 µm and refractive index of pure water, $m=1.33-0i$, is used for particles of diameter larger than 2 µm, which are mainly fog droplets

Table 3
Parameters of the log-normal multimodal distribution approximating the particle size distribution in the clear-sky and haze regimes as well as during the first fog development stage: geometric mean diameter D_g, geometric standard deviation s_g, and number N per mode.

	Nucleation mode			Aitken mode			Accumulation mode			Fog droplet mode		
	N_{Nucl} (cm^{-3})	$D_{g,Nucl}$ (µm)	$s_{g,Nucl}$	N_{Aitk} (cm^{-3})	$D_{g,Aitk}$ (µm)	$s_{g,itk}$	N_{acc} (cm^{-3})	$D_{g,acc}$ (µm)	$s_{g,acc}$	N_{fd} (cm^{-3})	$D_{g,fd}$ (µm)	$s_{g,fd}$
Unpolluted clear-sky	1000	0.02 ± 0.01	1.5 ± 0.2	4000	0.08 ± 0.01	1.8 ± 0.2	20–60	0.5 ± 0.3	1.7 ± 0.3	/	/	/
Transport of pollution	2000–6000	0.02 ± 0.01	1.6 ± 0.1	6000–11000	0.08 ± 0.01	1.8 ± 0.1	100	0.5 ± 0.3	1.7 ± 0.1	/	/	/
Haze	8000	0.03±0.01	1.6±0.1	11000	0.09±0.01	1.6±0.1	100–3000	0.6±0.1	1.4±0.1	/	/	/
Fog	2000–6000	0.04 ± 0.01	1.6 ± 0.2	5000–8000	0.11 ± 0.02	1.6 ± 0.1	4500	0.8 ± 0.1	1.4 ± 0.1	700	3.2 ± 0.2	1.5 ± 0.1

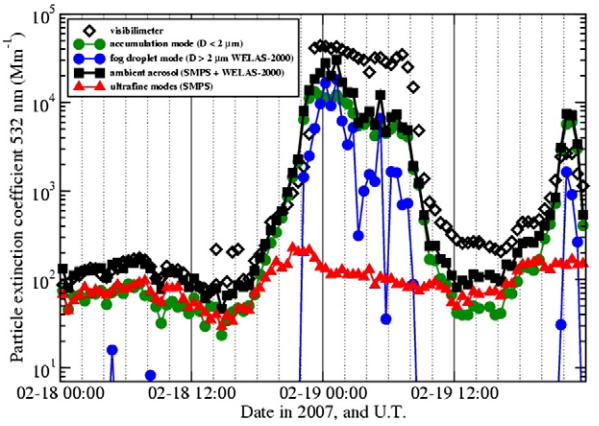

Fig. 5. Time series of particle extinction coefficients derived by Mie theory for different particle populations (Eq. (4a)) and derived by the Koschmieder equation and the visibilimeter measurements (Eq. (3)).

and wet aerosol particles. D_{min} is 0.01 μm and D_{max} is 42 μm. 30% uncertainty is estimated on σ^{M}_{ext}, taking into account the instrumental errors, the uncertainties from the two systems to provide the size distribution and the assumptions used in the optical property algorithm. Extinction coefficient is also computed for different aerosol populations, with $D_{min}=0.01$ μm and $D_{max}=0.40$ μm to represent the ultrafine aerosol contribution $\Delta_{uf}\sigma^{M}_{ext}$, with $D_{min}=0.4$ μm and $D_{max}=2$ μm to represent the accumulation mode contribution $\Delta_{acc}\sigma^{M}_{ext}$, and with $D_{min}=2$ μm and $D_{max}=42$ μm to represent fog droplet mode contribution $\Delta_{fd}\sigma^{M}_{ext}$. They are related as $\Delta_{uf}\sigma^{M}_{ext}+\Delta_{acc}\sigma^{M}_{ext}+\Delta_{fd}\sigma^{M}_{ext}=\sigma^{M}_{ext}$. Time series of the extinction coefficients are plotted in Fig. 5.

The angularly-truncated scattering coefficient is also computed using the SMPS size distribution, in order to compare with the nephelometer measurements $\sigma^{N}_{scat}(\lambda)$, as:

$$\Delta_{uf}\sigma^{M}_{scat}(\lambda)=\frac{\int_{7^\circ}^{170^\circ}p(\Theta,\lambda)d\Theta}{\int_{0}^{180^\circ}p(\Theta,\lambda)d\Theta}\sum_{D_{min}}^{D_{max}}\frac{\pi D^2}{4}\Delta n(D)Q_{scat}(m,D,\lambda) \quad (4b)$$

Where $p(\Theta,\lambda)$ is the phase function describing the angular dependence of particle scattering, computed according to Mie theory as a function of the wavelength λ and the scattering angle Θ. $Q_{scat}(m, D, \lambda)$ is the Mie scattering efficiency factor. D_{min} is 0.01 μm and D_{max} is 0.50 μm, and λ is 450, 550 and 700 nm. Time series of $\Delta_{uf}\sigma^{M}_{scat}(\lambda)$ are plotted in Fig. 6, together with the scattering coefficient $\sigma^{N}_{scat}(\lambda)$ directly measured by the nephelometer.

Column Ångström exponent α_{col} is computed considering the measurements of aerosol optical thickness made at four wavelengths (e.g. Holben et al., 2001) during the day by the CE318 sunphotometer. Similarly, surface nephelometer Ångström exponent α^{N}_{surf} is estimated using the scattering coefficient measured at three wavelengths by the nephelometer, and surface Mie Ångström exponent α^{M}_{surf} computed with the generated ambient size distribution.

4. The clear-sky regime

Clear-sky regime is defined arbitrarily for visibility larger than 5000 m, in contrast to hazy and foggy conditions when visibility can reach dramatically smaller values. Two situations are observed during the clear-sky regime. The first situation is relatively stable in terms of visibility, when variability in visibility is mainly due to changes of the atmospheric boundary layer height: visibility ranges between 15 000 and 35 000 m during the 17–18/02 night and the 18/02 day (classified as "quasi-clear" by Jiusto, 1981), and around 10 000 m on 19/02 mid day. The second situation is a steady decrease or increase in visibility, as from 30 000 to 8000 m on 18/02 afternoon, because of squeezing of the boundary layer and because of advected pollution particles after a change in the wind direction. Aerosol properties are described in detail in the following.

4.1. The ambient aerosol size distribution

Koschmieder-estimate σ^{K}_{ext} and Mie-estimate σ^{M}_{ext} of the extinction coefficient agree during the 18 February clear-sky regime (Fig. 5). In particular, minimum and maximum values of the extinction coefficient are reproduced: diurnal minimum of around 70 Mm^{-1} is reached between 1300 and 1500 UT, corresponding to the warmest time of the day (Fig. 1); diurnal maximum of 180 Mm^{-1} is reached around 0715 UT when temperature is minimum at 1, 2, and 5 m agl. The decrease of σ^{K}_{ext} by 80 Mm^{-1} from 0715 UT to 0915 UT, observed by the visibilimeter, is also reproduced by microphysical measurements. Similar values, included between 80 and 100 Mm^{-1}, were observed on 31 July 2000 at ground level in the Paris area (Chazette et al., 2005). Column and surface Ångström exponents also agree on 18 February, with α_{col} included between 0.6 and 1.0, and α^{M}_{surf} similarly included between 0.2 and 0.9.

Moreover both methods agree to indicate the increase of extinction coefficient from $\sigma^{K}_{ext}=100$ Mm^{-1}, starting at 1745 UT, that coincides with a change in the wind direction from West to East: urban pollution is advected to the site. The extinction coefficient increases up to 400 Mm^{-1} (equivalent to visibility smaller than 10 000 m) because of pollution particles. It remains

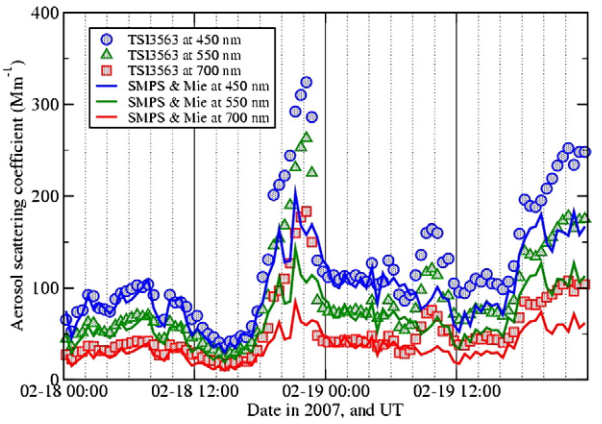

Fig. 6. Time series of the angularly-truncated scattering coefficient at three wavelengths, measured directly by the TSI-3563 nephelometer and computed according to Mie theory applied on aerosol size distribution measured by the TSI SMPS particle counter.

still smaller than what is observed in the Po Valley during the CHEMDROP experiment (Yuskiewicz et al., 1998), when the scattering coefficient generated by all particles is 900 Mm^{-1}.

Agreement on 18/02 validates the set of aerosol parameters composed by the size distribution and the refractive index. In contrary, the size distribution measured on 19/02 cannot be used as microphysical measurements underestimate the extinction coefficient by a factor 2 to 3, beyond uncertainty range, even if variability is reproduced, such as the decrease in extinction from 1015 to 1215 UT 19/02 and the increase from 1615 UT to 1815 UT. The clear-sky regime of 19/02 is quite different to that of 18/02, as visibility remains smaller than 14000 m and relative humidity is larger than 75%.

Aerosol size distribution measured in the 18/02 clear-sky regime can be approximated by a trimodal log-normal distribution (bimodal from SMPS measurements and monomodal from WELAS-2000) (Table 3). Ultrafine aerosol particles are distributed in the nucleation mode located around 0.02 μm diameter and in the Aitken mode located around 0.08 μm. Yuskiewicz et al. (1998) estimate an Aitken mode diameter included between 0.09 and 0.15 μm in dry conditions. Accuracy on the accumulation mode diameter is poor as aerosol number is relatively small. It is located between 0.2 and 0.8 μm, consistently with Yuskiewicz et al. (1998) providing the value of 0.4 μm, and with Randriamiarisoa et al. (2006) estimating accumulation mode diameter around 0.2 μm, and a further mode beyond 0.8 μm.

4.2. The ultrafine mode aerosol properties

Scattering coefficient measured by the nephelometer $\sigma^{N}_{scat}(\lambda)$ is used to validate the properties of the ultrafine mode of the aerosol size distribution measured by the SMPS in clear-sky regime. $\sigma^{N}_{scat}(\lambda)$ and $\Delta_{uf}\sigma^{M}_{scat}(\lambda)$ are sensitive to dynamic processes and thermodynamic conditions of the boundary layer on 18/02 as they both show similar features to σ^{K}_{ext} and σ^{M}_{ext}. For example, on 18/02, $\sigma^{N}_{scat}(\lambda=550\ nm)$ is maximum at 0745 UT, with 70 Mm^{-1} (Fig. 6) and is minimum at 1445 UT, with 25 Mm^{-1}. While $\Delta_{uf}\sigma^{M}_{scat}(\lambda)$ and $\sigma^{N}_{scat}(\lambda)$ agree at 450 nm within uncertainties, $\Delta_{uf}\sigma^{M}_{scat}(\lambda)$ is smaller than $\sigma^{N}_{scat}(\lambda)$ at 700 nm because of particles larger than 0.5 μm, which are outside the SMPS size domain but sounded by the nephelometer. As scattering efficiency depends on particle size (e.g. Bohren and Huffman, 1983), contribution to scattering by these particles is more important at 700 than at 450 nm. These particles seem more numerous on 19/02 afternoon as underestimation is observed at all wavelengths (and still stronger at 700 nm). The diurnal clear-sky regime of 18/02 can be classified as continental background (Elias et al., 2006), in regards to the in situ optical measurements and also to the aerosol optical thickness ranging between 0.15 and 0.27 at 440 nm. Aerosol number of around 5000 cm^{-3} corresponds to values observed upstream Paris by an airborne instrument (Chazette et al., 2005), as $4600\pm1500\ cm^{-3}$. Scattering coefficient data are also included in the range of values observed in North Atlantic Ocean (Hoppel et al., 1990; Hegg et al., 1993, 1995). Agreement between computations and measurements provide the validation of the data set. Consequently, aerosol size distributions can be used to correct precisely measured scattering coefficient by the angular truncation.

Change in the wind direction causes an increase of $\sigma^{N}_{scat}(\lambda)$ by a factor 2 that consequently reaches 90 Mm^{-1} at 550 nm due to pollution. During the clear-sky regime, the aerosol number varies between 3900 and 11300 cm^{-3}, and it reaches 19000 cm^{-3} under the East wind regime. The aerosol load reaches levels observed in the Po Valley by Noone et al. (1992), with values included between 17000 and 25000 cm^{-3}, and by Yuskiewicz et al. (1998) with values included between 4000 and 40000 cm^{-3} during the CHEMDROP experiment. Proportion of nucleation mode aerosols increases, as the nucleation mode number is multiplied by 6 while the Aitken mode number is multiplied by 3 (Table 3). This is confirmed by the difference observed between N_C and N_S during the change in the wind pattern, certainly due to aerosol particles included between 0.004 and 0.010 μm diameter.

4.3. Accumulation mode aerosols

The difference between σ^{K}_{ext} and $\sigma^{N}_{scat}(\lambda=550\ nm)$ is partly due to aerosol absorption and to angular truncation effect, jointly estimated to provide less than 20% difference. Thus the observed factor 2 difference indicates that aerosol particles larger than 0.5 μm, distributed in the accumulation mode, do not pass through the PM10 inlet while they do contribute strongly to extinction of visible radiation. Unpolluted clear-sky maximum in accumulation mode number is reached at 0715 UT with 60 cm^{-3}, while the minimum occurs at 1445 UT with 20 cm^{-3}. All features showed by $\Delta_{acc}\sigma^{M}_{ext}$, are also observed in time series of σ^{K}_{ext}, σ^{M}_{ext}, σ^{N}_{scat} and $\Delta_{uf}\sigma^{M}_{scat}$. According to Mie computations, the accumulation mode contributes by around 50% to particle extinction (Fig. 5), while the ultrafine modes contribute to the other half, even though the ultrafine aerosol particles are 100 times more numerous than the accumulation mode aerosol number. The accumulation mode contribution to extinction starts to overwhelm the ultrafine mode contribution after the change in the advection pattern, as this change causes a factor 4 increase in σ^{K}_{ext}, but a factor 2 increase in σ^{N}_{scat}.

5. Wet aerosol particles generating the haze regime

Haze is due to hydration of aerosol particles when relative humidity is beyond the deliquescence point. As activation is not engaged and no droplets are present, extinction is not spectrally neutral (Middleton, 1958; Eldridge, 1966). Haze regimes of 18–19/02 are characterised as: 1) visibility smaller than 5000 m; 2) strong temporal gradients in visibility and aerosol number, as relative humidity decreases or increases between 75 and 100%.

5.1. Evidence of engaged hydration process

Before 1700 UT 18/02, the accumulation mode aerosol number N_{acc} is smaller than 60 cm^{-3}, and the ultrafine mode aerosol number N_S is smaller than 12000 cm^{-3} (Fig. 3), both modes generating a visibility included between 16000 and 35000 m (Fig. 2). The wind starts changing direction at sunset, at 1710 UT (RH = 70%). N_S increases by a factor 2 and N_{acc} increases by a factor 4 in 2 h while the wind direction continues to change. At 1850 UT when the wind direction is stabilized to the East, indicating air masses coming from

polluted zones, visibility has already decreased down to 7700 m (RH = 90%). N_S reaches a plateau around 19 000 cm^{-3} while N_{acc} continues increasing from 150 to 5200 cm^{-3} in less than 4 h (N_{acc} = 400 cm^{-3} when visibility is 5000 m). The divergence between N_S and N_{acc} after 1850 UT indicates that the cause of N_{acc} increase is not advective, but may be due to water uptake by aerosol particles, with relative humidity increasing simultaneously from 90 to 100%. Due to hydration aerosol, particles initially smaller than 0.39 μm grow and reach the WELAS-2000 size detection domain. The reservoir of ultrafine mode aerosols is sufficient to provide the measured increase of wet aerosol number. Equal decrease in ultrafine mode aerosol number is not noticed because it can be partly compensated by the boundary layer shrinking.

5.2. Effect on ultra-fine aerosol size distribution

Ultrafine aerosol integrated number is not affected by the hydration process but comparison of nephelometer and SMPS measurements indicate that the ultrafine aerosol size distribution varies. Start of increase of ultrafine mode aerosol number N_S at 1625 UT, from 5400 cm^{-3}, coincides with the start of increase of scattering coefficient σ^N_{scat} from 45 Mm^{-1} at 450 nm. However maxima in N_S (Fig. 3) and σ^N_{scat} (Fig. 6) do not coincide in time, indicating a change in the aerosol size distribution, i.e. the proportion of largest particles entering the nephelometer increases while N_S remains relatively constant, generating a maximum in σ^N_{scat} later than the N_S maximum. From the start of particle hydration process, SMPS underestimates nephelometer measurements, indicating significant contribution to scattering by particles larger than 0.5 μm. This is confirmed by the scattering Ångström exponent α^N_{surf} measured by the nephelometer, which is included between 1.2 and 1.6 from 2015 UT to 2245 UT while it is relatively constant between 1.8 and 2.0 during the 18/02 clear-sky regime. α^N_{surf} also decreases significantly during the post-fog haze. Log-normal fitting confirms the change in the size distribution, as a shift of both ultra-fine modes to larger sizes. Between 1915 and 2015 UT, nucleation mode diameter increases from 0.02 to 0.03 μm and the Aitken mode diameter increases from 0.08 to 0.10 μm, while both mode numbers remain constant around 8000 and 11000 cm^{-3}, respectively (Table 3).

To show the aerosol sensitivity to relative humidity, aerosol scattering cross section is computed by dividing aerosol scattering coefficient by the aerosol number (Randriamiarisoa et al., 2006), both derived from aerosol size distributions measured by SMPS on 18/02. Aerosol scattering cross section is then independent on particle transport. The aerosol scattering cross section is plotted for both decreasing and increasing relative humidity regimes in Fig. 7. The scattering growth coefficient γ (Hänel, 1976) representing the sensitivity of the scattering coefficient to relative humidity, is estimated around 0.6 for the increasing relative humidity regime, occurring when the site is under easterly winds loaded with pollution aerosols.

5.3. Contribution to extinction by accumulation mode aerosols

Measurements agree to indicate that wet aerosol particles distributed in the accumulation mode are the main contributors to haze extinction, on 18 and 19 February. From the change in the advection pattern, the accumulation mode contribution to extinction increases, from 50% in the clear-sky regime to 100% around 2200 UT. Just before the fog outbreak, Mie-estimate overestimates visibilimeter-estimate. N_{acc} varies between 400 and 5200 cm^{-3} in the haze, which is consistent with observations of 2000 cm^{-3} aerosol particles at 1200 m visibility made by Eldridge (1966). Meanwhile, accumulation mode diameter stabilises around 0.60 μm.

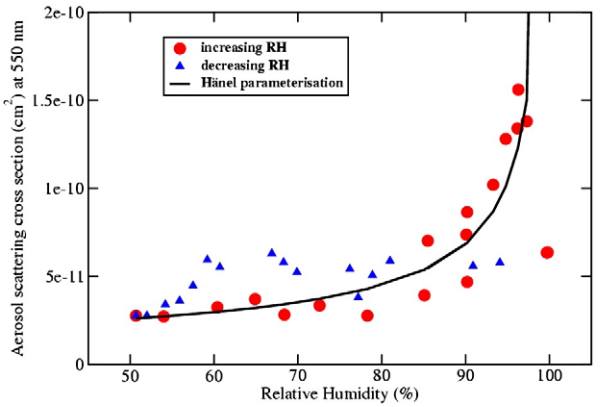

Fig. 7. Aerosol scattering cross-section (cm^2) estimated at 550 nm from Mie theory applied on SMPS measurements made on 18 February, for both increasing and decreasing relative humidity (RH) regimes. The line shows a parameterisation with the scattering growth coefficient γ = 0.6 (Hänel, 1976).

6. Extinction in fog

Aerosol activation is the process leading to fog formation. The diameter range of particles co-existing in the atmosphere is extending in fog conditions, with simultaneous presence of droplets and interstitial aerosol particles. In terms of the extinction properties, stabilisation is reached for 10 h in fog, with visibility of 100 ± 45 m. Visibility signal is observed at 400 m visibility, with 97% relative humidity at 1 and 30 m agl. Given a few % uncertainty, the atmosphere is indeed saturated in humidity. Three stages may be observed in the fog development, in regards to variability of visibility. The first stage consists in constant visibility around 70 m, for a duration of 2.5 h. The second stage is a transition phase, characterised by a steady increase of visibility from 70 to 110 m in 2 h. During the third stage, the variability increases from 80 to 180 m, intermittently in more than 4 h. Particle microphysics and optics are discussed thereafter.

6.1. Interstitial aerosol particles: ultrafine and accumulation modes

No particles of diameter larger than 0.50 μm enter the PM10 inlet in fog regime, as demonstrates the agreement between measured and computed scattering coefficients (Fig. 6). Consequently, the Ångström exponent α^N_{surf} reaches largest values (from 2.0 to 2.5) within the fog. Moreover smallest aerosol particles are lost due to collisions, causing a decrease of N_S from 15 300 cm^{-3} to 7100 cm^{-3} during the first fog development stage, while σ^N_{scat} remains almost unaffected. The nucleation mode number drops down from 8000

to 2000 cm^{-3}, while the Aitken mode number decreases by a factor 2 only (Table 3).

The ultrafine mode contribution to fog extinction is negligible: values of $\Delta_{uf}\sigma^{M}_{ext}$ during the third fog stage are very close to values in clear-sky conditions. However contribution to extinction by accumulation mode, $\Delta_{acc}\sigma^{M}_{ext}$, is not negligible in the fog. Accumulation mode contribution to extinction remains larger than 11 200 Mm^{-1} during the first fog development stage, with N_{acc} stabilised above 4300 cm^{-3}, and maximum at 5700 cm^{-3} reached at 2315 UT. In this case, contribution to extinction by accumulation mode can be estimated by 30%, however considering that DF320 extinction coefficient is overestimated by microphysics-estimate before fog onset, another estimate of 10% is obtained by extrapolating DF320 extinction coefficient measured before droplet formation within the fog. Final estimate of the accumulation mode contribution to extinction is then $20 \pm 10\%$. Mode diameter increases from 0.60 to 0.90 μm in the first stage and decreases back from 0.90 to 0.60 μm in the third stage. $\Delta_{acc}\sigma^{M}_{ext}$ stabilises between 4400 and 6700 Mm^{-1} during the third stage, with N_{acc} included between 1500 and 3300 cm^{-3}.

6.2. Measurement of fog droplets

Fog is clearly linked to presence of droplets larger than 2 μm (Figs. 4 and 5, and Table 2), cause of the neutral spectral dependence of light extinction. Considering the threshold in fog droplet number of 100 cm^{-3}, deduced from the definition of the mist transition phase between haze and fog (Heintzenberg et al., 1998), first droplets appear at 2225 UT, 20 min before the visibility signal (Section 2.2). Relative humidity is 97% and visibility is 1200 m, outside the value interval defined by Eldridge (1969) for the mist regime, but agrees with Meyer et al. (1980). From then and until the third fog development stage, accumulation mode number is larger than 3000 cm^{-3}, and $\Delta_{acc}\sigma^{M}_{ext}$ is larger than 5000 Mm^{-1}. However the number of fog droplets is not stabilised until measured relative humidity reaches 99% at 1 m agl, at 2255 UT. Indeed N_{fd} varies between 120 and 380 cm^{-3} between 2225 and 2245 UT, and decreases back below 100 cm^{-3} at 2250 UT. From 2255 UT on, N_{fd} is larger than 150 cm^{-3}. Similarly, the accumulation mode number is larger than 4500 cm^{-3} from 2255 UT, while it is 3000 cm^{-3} at 2250 UT.

The ambient particle size distribution best reproduces fog extinction during the first fog stage at 0015 and 0115 UT when $\sigma^{M}_{ext} = 30\,000$ Mm^{-1} (Table 2): σ^{K}_{ext} agrees with σ^{M}_{ext}, within aggregated uncertainties, as $\sigma^{M}_{ext}/\sigma^{K}_{ext} = 0.7$. The order of magnitude of the contribution to extinction by fog droplets, $\Delta_{fd}\sigma^{M}_{ext}$, is similar to the accumulation contribution, during the entire first stage. $\Delta_{fd}\sigma^{M}_{ext}$ is larger than 5200 Mm^{-1}, and reaches its maximum of 19300 Mm^{-1} at 0115 UT, when N_{fd} also reaches its maximum of 700 cm^{-3}. WELAS-2000 measurements made at 0015 and 0115 UT are used to get log-normal mode parameters approximating the particle size distribution in fog conditions (Table 3). According to measurements, fog droplets are distributed in a unique mode, with a mean diameter of around 3.2 μm. Eldridge (1966) and Meyer et al. (1980) observe modes of fog droplets at 3 and 10 μm diameter. Heintzenberg et al. (1998) observe a mode at around 6 μm, but they attribute it to haze conditions. Assuming the solid part of the droplets is negligible, integrated volume provides the liquid water content (LWC), which reaches maximum of 30 mg m^{-3}, according to the WELAS-2000 measurements. According to literature, this value is too small. For example Eldridge (1966) reports value of LWC larger than 95 mg m^{-3} for visibility range smaller than 100 m.

Comparison of extinction coefficient during the third stage of the fog shows a deficit in counted particles. It is deduced that these particles are fog droplets larger than 10 μm diameter. Indeed, contribution by Aitken mode is negligible in fog. Contribution to extinction by the accumulation mode follows the variability of visibility observed during each stage of the fog, while contribution to extinction by fog droplets of diameter larger than 2 μm seems erratic, especially in the third fog stage. In the second and third stages, $\Delta_{fd}\sigma^{M}_{ext}$ is highly variable while both accumulation mode contribution and measured visibility remain relatively constant (Fig. 5). Moreover $\Delta_{fd}\sigma^{M}_{ext}$ can be as small as 50 Mm^{-1}, even if both visibilimeters indicate presence of a dense fog. Meyer et al. (1980) suspect a mode at 20 μm, which is effectively observed by Heintzenberg et al. (1998), leading to validation of the size distribution with independent extinction measurements (Yuskiewicz et al., 1998). Such mode would indeed increase fog extinction and LWC both computed in this study. Observed third fog development stage might correspond to the mass transfer phase observed by Wendisch et al. (1998), characterised by a drastically rise of large droplet number, and quasi-periodic oscillations in data. Four to five such oscillations of around 40-minute period might be observed between 0400 and 0700 UT in the time series of temperature (Fig. 1), visibility and WELAS-2000 particle number (on a 5-minute temporal resolution, not showed here).

7. Conclusion

This paper presents the exploitation of the data set acquired during the ParisFog field experiment, dedicated to describe the role of radiative, dynamic and thermodynamic processes during a fog life cycle, in connection with the microphysical properties of aerosol particles and fog droplets. The case study concerns a dense and homogeneous fog formed from nocturnal radiative cooling in a polluted environment. According to both the horizontal visibility range and the accumulation mode aerosol number, three regimes are identified, clear-sky, haze and fog, as well as three fog development stages. This study shows the consistency of the experimental set-up for measuring aerosol optical and microphysical properties in variable conditions of atmospheric humidity: relative humidity changes between 50 and 100%, visibility ranges between 65 and 35 000, the site is either downwind Paris urban area either under maritime influence. The experimental set-up provides insights about the sensitivity of microphysical and optical properties of several particle populations, all contributing to atmospheric extinction of visible radiation, to: 1) the surface layer temperature, 2) relative humidity; and 3) atmospheric dynamics.

The seven particle-dedicated in-situ instruments agree for the time of the minimum and the maximum values of the aerosol load and extinction/scattering coefficient, at surface level and during the 18/02 unpolluted clear-sky regime. Such aerosol properties are affected by the height of the atmospheric

boundary layer, which depends on the temperature. Moreover all instruments provide a signal of the change in the air mass origin, when the wind direction changes from West to East. More specifically, the Degreanne visibilimeters as well as the PALAS WELAS-2000 are indicative of the changes of regimes, and are both indicative of the stages in fog development. Besides, the TSI SMPS and GRIMM CPC particle counters and the TSI-3563 nephelometer are indicative of the changes in the aerosol sources.

Quantitative comparison between sets of measurements are run by performing computations of optical properties, according to Mie theory applied on measurements of microphysical properties. Two sets of comparisons are performed, according to the sampling conditions. Measurements made downstream the PM10 inlet, by the SMPS particle counter as well as by the nephelometer, are consistent with each other, within combined uncertainties, in dry unpolluted and polluted clear-sky, and in fog regimes. Measurements made in ambient conditions by the WELAS-2000 and the visibilimeters are consistent, within combined uncertainties, in dry unpolluted and polluted clear-sky conditions and also in the first fog development stage. These agreements provide validation of the parameter sets describing the particle microphysical and optical properties during these particular conditions. Size distributions are composed by several modes corresponding to different particle populations: nucleation mode and Aitken aerosol particles, dry and wet accumulation mode aerosols, and fog droplets. Contribution to extinction by accumulation mode aerosols is significant in all regimes: from haze (100%) to clear-sky (50%) and to fog conditions ($20 \pm 10\%$).

Ultrafine modes contribute by 50% to extinction of visible radiation during the dry clear-sky regime, which is typical of European continental background. Eastern winds bring ultrafine aerosol particles from the Paris area after sunset, the Aitken mode number increasing by a factor 2 and the nucleation mode number increasing by a factor 4. The nucleation aerosol particles are then mainly lost by collisions with droplets, their number falling down by a factor 3 in fog. In clear-sky conditions, few particles do not go through the PM10 inlet, but they are highly effective in contributing to extinction. They are distributed in the accumulation mode defined by a geometric mean diameter included between 0.2 and 0.8 μm, with N_{acc} included between 20 and 60 cm^{-3}. Their number increases by a factor 30 due first to air mass advection and second to the hydration process when relative humidity is larger than the deliquescence point, consequently generating the haze. Observations indicate that hydration process is already engaged at visibility of 7700 m, which shows that 5000 m is an arbitrary threshold which could be refined. Moreover formation of fog droplets creates a signal on the time series of visibility. Therefore the fog onset is identified by the maximum in the temporal gradient of visibility, as well as the fog dissipation, occurring respectively at a visibility of 400 m and 880 m.

In terms of extinction, only the accumulation and droplet modes are significant in fog. The accumulation mode of wet aerosol particles contributes to $20 \pm 10\%$ extinction by the fog, with an aerosol number of around 4500 cm^{-3} during first stage of fog development. Wet aerosol particles are distributed around the mean geometric diameter $D_{g,acc} = 0.8$ μm with a geometric standard deviation of $s_{g,acc} = 1.4$. Wet aerosol number decreases during the second stage and remains included between 1500 and 3400 cm^{-3} in the third stage, still contributing to around 20–30% extinction in the fog, according to WELAS-2000. Consequently existing parameterisations of visibility in function of particle number (Gultepe et al., 2006) may be improved by considering aerosol particles smaller than 2 μm diameter. A droplet mode is observed during the first fog development stage, distributed around the geometric mean diameter $D_{g,fd} = 3.2$ μm, with a geometric standard deviation $s_{g,fd} = 1.5$, which contributes by 40% to extinction in the fog. 30% missing extinction lies within uncertainties. It is assumed that droplet counts are missing during the second and third development stages. Missing droplet mode could lie for diameter larger than 10 μm.

This study provides the validation of microphysical characteristics of particles while thermodynamic and dynamic processes cause high variations in visibility range. By associating radiative transfer computations and supplementary measurements of radiative properties of the atmospheric surface layer, further step will consist in studying the implication of particle properties in fog life cycle: 1) effect of particles on radiative cooling of the surface; 2) contributions of the different aerosol populations in absorption and extinction of solar radiation leading to fog dissipation.

Acknowledgements

Authors are very grateful to all site operators, meteorology forecasters, instrument owners, database managers who participated to the ParisFog field campaign. AERONET is also acknowledged for the sunphotometer data.

References

Anderson, T., Covert, D., Marshall, S., Laucks, M., Charlson, R., Waggoner, A., Ogren, J., Caldow, R., Holm, R., Quant, F., Sem, G., Wiedensohler, A., Ahlquist, N., Bates, T., 1996. Performance characteristics of a high-sensitivity, three-wavelength, total scatter/backscatter nephelometer. J. Atmos. Oceanic Technol. 13, 967–986.

Bergot, T., Haeffelin, M., et al., 2008. ParisFog: des chercheurs dans le brouillard. La Météorologie 62.

Bohren, C.F., Huffman, D.R., 1983. Absorption and Scattering of Light by Small Particles. John Wiley, New York.

Chazette, P., Randriamiarisoa, H., Sanak, J., Couvert, P., Flamant, C., 2005. Optical properties of urban aerosol from airborne and ground based in situ measurements performed during the ESQUIF program. J. Geophys. Res. 110, D02206. doi:10.1029/2004JD004810.

Eldridge, R.G., 1966. Haze and fog distributions. J. Atmos. Sci. 23, 605–613.

Eldridge, R.G., 1969. Mist — the transition from haze to fog. Bull. Amer. Met. Soc. 50, 422–426.

Elias, T., Silva, A.M., Belo, N., Pereira, S., Formenti, P., Helas, G., Wagner, F., 2006. Aerosol extinction in a remote continental region of the Iberian peninsula during summer. J. Geophys. Res. 111, D14204. doi:10.1029/2005JD00.

Fuzzi, S., Laj, P., Ricci, L., Orsi, G., Heintzenberg, J., Wendisch, M., Yuskiewicz, B., Mertes, S., Orsini, D., Schwanz, M., Wiedensohler, A., Stratmann, F., Berg, O.H., Swietlicki, E., Frank, G., Martinsson, B.G., Günther, A., Dierssen, J.P., Schell, D., Jaeschke, W., Berner, A., Dusek, U., GalamboS, Z., Kruisz, C., Mesfin, N.S., Wobrock, W., Arends, B., Ten, B.H., 1998. Overview of the Po Valley fog experiment 1994 (CHEMDROP). Contr. Atmos. Phys. 71, 3–19.

Gultepe, I., Müller, M.D., Boybeyi, Z., 2006. A new visibility parameterization for warm-fog applications in numerical weather prediction models. J. Appl. Meteor. Climatol. 45, 1469–1480.

Haeffelin, M., Barthès, L., Bock, O., Boitel, C., Bony, S., Bouniol, D., Chepfer, H., Chiriaco, M., Cuesta, J., Delanoe, J., Drobinski, P., Dufresne, J.L., Flamant, C., Grall, M., Hodzic, A., Hourdin, F., Lapouge, F., Lemaitre, Y., Mathieu, A.,

Morille, Y., Naud, C., Noel, V., OH'irok, B., Pelon, J., Pietras, C., Protat, A., Romand, B., Scialom, G., Vautard, R., 2005. SIRTA, a ground-based atmospheric observatory for cloud and aerosol research. Ann. Geophys. 23, 253–275.
Hänel, G., 1976. The properties of atmospheric aerosol particles as functions of the relative humidity at thermodynamic equilibrium with the surrounding moist air. Adv. Geophys. 19, 73–188.
Hegg, D.A., Ferek, R.J., Hobbs, P.V., 1993. Light scattering and cloud condensation nucleus activity of sulphate aerosol measured over the Northeast Atlantic Ocean. J. Geophys. Res. 98 (D8), 14 887–14 894.
Hegg, D.A., Hobbs, P.V., Ferek, R.J., Waggoner, A.P., 1995. Measurements of some aerosol properties relevant to radiative forcing on the east coast of the United States. J. Appl. Meteorol. 34, 2306–2315.
Heintzenberg, J., 1994. Properties of the log-normal particle size distribution. Aerosol Sci. Technol. 21, 46–48.
Heintzenberg, J., Wendisch, M., Yuskiewicz, B., Orsini, D., Wiedensohler, A., Stratmann, F., Frank, G., Martinsson, B.G., Schell, D., Fuzzi, S., Orsi, G., 1998. Characteristics of haze, mist and fog. Contr. Atmos. Phys. 71, 21–31.
Hess, M., Koepke, P., Schult, I., 1998. Optical properties of aerosols and clouds: the software package OPAC. Bull. Am. Meteorol. Soc. 79 (5), 831–844.
Holben, B.N., Eck, T.F., Slutsker, I., Tanré, D., Buis, J.P., Setzer, A., Vermote, E., Reagan, J.A., Kaufman, Y.J., Nakajima, T., Lavenu, F., Jankowiak, I., Smirnov, A., 1998. AERONET — a federated instrument network and data archive for aerosol characterization. Remote Sens. Environ. 66, 1–16.
Holben, B.N., Tanré, D., Smirnov, A., Eck, T.F., Slutsker, I., Abuhassan, N., Newcomb, W.W., Schafer, J., Chatenet, B., Lavenue, F., Kaufman, Y.J., Vande Castle, J., Setzer, A., Markham, B., Clark, D., Frouin, R., Halthore, R., Karnieli, A., O'Neill, N.T., Pietras, C., Pinker, R.T., Voss, K., Zibordi, G., 2001. An emerging ground-based aerosol climatology: aerosol optical depth from AERONET. J. Geophys. Res. 106, 12 067–12 097.
Hoppel, W.A., Fitzgerald, J.W., Frick, G.M., Larson, R.E., Mack, E.J., 1990. Aerosol size distributions and optical properties found in the marine boundary layer over the Atlantic Ocean. J. Geophys. Res. 95 (D4), 3659–3686.
Jiusto, J.E., 1981. Fog structure. In: Hobbs, P.V., Deepak, A. (Eds.), Clouds: Their Formation, Optical Properties and Effects. Academic Press, New York, pp. 187–239.
Koschmieder, H. Theorie der horizontalen Sichtweite, Beitraege Physicae Freiberger Atmosphere, 12, 33–55, 171–181, 1925.
Kunkel, B.A., 1984. Parameterization of droplet terminal velocity and extinction coefficient in fog models. J. Clim. Appl. Meteorol. 23, 34–41.
Meyer, M.B., Jiusto, J.E., Lala, G.G., 1980. Measurements of visual range and radiation-fog (haze) microphysics. J. Atmos. Sci. 37, 622–629.
Middleton, W.E.K., 1958. Vision Through the Atmosphere. University of Toronto Press, Toronto.
National Oceanic and Atmospheric Administration, 1995. Surface weather observations and reports. Federal Meteorological Handbook, vol. 1. 94 pp.
Noone, K.J., Ogren, J.A., Hallberg, A., Heintzenberg, J., Ström, J., Hansson, H.C., Svenningsson, B., Wiedensohler, A., Fuzzi, S., Facchini, M.C., Arends, B.G., Berner, A., 1992. Changes in aerosol size- and phase distributions due to physical and chemical processes in fog. Tellus 44B, 489–504.
Randriamiarisoa, H., Chazette, P., Couvert, P., Sanak, J., Mégie, G., 2006. Relative humidity impact on aerosol parameters in a Paris suburban area. Atmos. Chem. Phys. 6, 1389–1407.
Seinfeld, J.H., Pandis, S.N., 1998. Atmospheric Chemistry and Physics: From Air Pollution to Climate Change. John Wiley, New York. 1360 pp.
Shettle, E.P., Fenn, R.W., 1979. Models for the aerosols of the lower atmosphere and the effects of humidity variations on their optical properties, AFGL-TR-79-0214, 94 pp.
Tardif, R., Rasmussen, R.M., 2007. Event-based climatology and typology of fog in the New York City region. J. Appl. Meteor. Climatol. 46, 1141–1168.
Vautard, R., Menut, L., Beekmann, M., Chazette, P., Flamant, P.H., Gombert, D., Guedalia, D., Kley, D., Lefebvre, M.P., Martin, D., Mégie, G., Perros, P., Toupance, G., 2003. A synthesis of the air pollution over the Paris region (ESQUIF) field campaign. J. Geophys. Res. 108 (D17), 8558. doi:10.1029/2003JD003380.
Wendisch, M., Mertes, S., Heintzenberg, J., Wiedensohler, A., Schell, D., Wobrock, W., Frank, G., Martinsson, B.G., Fuzzi, S., Orsi, G., Kos, G., Berner, A., 1998. Drop size distribution and LWC in Po Valley fog. Contr. Atmos. Phys. 71, 87–100.
Winkler, P., 1988. The growth of atmospheric aerosol particles with relative humidity. Phys. Scr. 37, 223–230.
Yuskiewicz, B., Orsini, D., Stratmann, F., Wendisch, M., Wiedensohler, A., Heintzenberg, J., Martinsson, B.G., Frank, G., Wobrock, W., Schell, D., 1998. Changes in submicrometer particle distributions and light scattering during haze and fog events in a highly polluted environment. Contr. Atmos. Phys. 71, 33–45.

List of acronyms

α^{M}_{surf}: Ångström exponent estimated by Mie theory applied on the ambient generated particle size distribution.
α^{N}_{surf}: Ångström exponent estimated from nephelometer measurements.
α_{col}: Ångström exponent estimated from sunphotometer measurements.
Agl: above ground level.
C_V: Visual contrast of the Koschmieder equation.
$\Delta_{uf/acc/fd}\,\sigma^{M}_{ext}$: ultrafine/accumulation/fog droplet mode contribution by Mie theory in the extinction coefficient (Mm^{-1}).
$\Delta_{uf}\sigma^{M}_{scat}$: ultrafine mode contribution by Mie theory in the scattering coefficient (Mm^{-1}).
$\Delta n\,(D)$: Particle size distribution (cm^{-3}).
ΔD: Size bin.
D_g: Geometric mean diameter of the log-normal mode (μm).
$D_{min/max}$: Minimum and maximum values of particle diameter (μm).
γ: Hänel scattering growth coefficient.
λ: Wavelength (nm).
LWC: Liquid Water Content ($mg\ m^{-3}$).
m: Particle refractive index.
$N_{acc/fd}$: Number of particles in the ultrafine/accumulation/fog droplet mode (cm^{-3}).
$N_{C/W}$: Aerosol number measured by the CPC/the SMPS/the WELAS-2000 (cm^{-3}).
N_S: Aerosol number measured by the SMPS, assimilated to the ultrafine mode number (cm^{-3}).
$p(\Theta,\lambda)$: Particle phase function depending on the scattering angle Θ and the wavelength λ.
$Q_{ext}(m,D)$, $Q_{scat}(m,D,\lambda)$: Mie extinction and scattering efficient factor.
RH: Relative humidity (%).
s_g: Geometric standard deviation of the log-normal mode.
$\sigma^{K/M}_{ext}$: Extinction coefficient estimated from the visibilimeter measurement/estimated from Mie theory applied on the particle size distribution measurements (Mm^{-1}).
$\sigma^{N}_{scat}(\lambda)$: Angularly-truncated scattering coefficient measured by the nephelometer (Mm^{-1}).
UT: Universal time.